SCIENCE CHINA
Chemistry

•REVIEWS•

October 2022 Vol.65 No.10: 1854–1866
https://doi.org/10.1007/s11426-022-1371-x

The contribution of water molecules to the hydrogen evolution reaction

Chao Cheng[1,2†], Mingming Deng[2†], Li Li[2*] & Zidong Wei[2*]

[1]*Chongqing Key Laboratory of Catalysis and New Environmental Materials, College of Environment and Resources, Chongqing Technology and Business University, Chongqing 400067, China;*
[2]*The State Key Laboratory of Power Transmission Equipment & System Security and New Technology, Chongqing Key Laboratory of Chemical Process for Clean Energy and Resource Utilization, College of Chemistry and Chemical Engineering, Chongqing University, Chongqing 400044, China*

Received July 1, 2022; accepted August 12, 2022; published online August 29, 2022

Traditionally, water molecules act as solvents in most chemical reactions, whereas they act as solvents and reactants in the alkaline electrolyte for the hydrogen evolution reaction (HER). It is well known that there is a current plateau in the linear potential–current dependence for HER in neutral or near-neutral electrolytes, showing that the HER is governed by the mass transport of reactive hydronium species at a given overpotential. The sharp rise in the current signal after the plateau at a slightly higher overpotential indicates that HER is supported by a new reactant, namely the water molecules rather than the limited hydronium species. Herein, in combination with our own research experience in water electrolysis, we review the relevant literature in these years about the HER activity descriptor and mainly focus on the contribution of water molecules to the HER, including their dissociation, configuration, and composition in regulating the pH-dependent HER. Finally, we try to provide new insights into understanding the mechanism of the HER in terms of interfacial water enrichment, orientation, and configuration with the electric field strength of electrode/electrolyte interface and electrode compositions.

water electrolysis, hydrogen evolution reaction, interfacial water

Citation: Cheng C, Deng M, Li L, Wei Z. The contribution of water molecules to the hydrogen evolution reaction. *Sci China Chem*, 2022, 65: 1854–1866, https://doi.org/10.1007/s11426-022-1371-x

1 Introduction

Water's structure and dynamic process at the solid–liquid interface are ubiquitous and play a crucial role across a broad spectrum in surface science, energy science, and catalysis [1–7]. One of the most fundamental issues in all these fields is the characterization of hydrogen evolution reaction (HER) on the cathode. HER is important in both technologies for improving the electrocatalytic behavior of electrode materials and the mechanism for developing the fundamental laws of modern electrochemistry concepts [8–14]. HER involves three possible steps, *i.e.*, Volmer step, Heyrovsky step, and Tafel step, in either acidic (reaction (1–3)) or alkaline (reaction (4–6)) solution. The difference is that the proton H^+ plays a reactant in acidic but H_2O in alkaline media. Anyway, the adsorbed hydrogen atom (H_{ad}) acts as the intermediate and plays a crucial role in determining the HER mechanisms [15–20]. The first step is the Volmer process forming hydrogen intermediates (H_{ad}). It is produced by H^+ accepting electrons in acidic (reaction (1)) media or water molecules accepting electrons as reactants in alkaline media (reaction (4)) [21,22]. In the second process of HER, gaseous hydrogen can be generated through the Tafel process (reaction (2) in acidic or (5) in alkaline media). Otherwise, the second electron transfers through the Heyrovsky process (reaction

†These authors contributed equally to this work
*Corresponding authors (email: liliracial@cqu.edu.cn; zdwei@cqu.edu.cn)

(3) in acidic or reaction (6) in alkaline media) [23–26]. The HER in acidic media, where water molecules act as solvents, and in alkaline media, where water molecules playing dual roles, reactants and solvents, are of fundamental importance for decades serving as model reactions for exploring the fundamental laws of electrocatalysis.

In acidic solutions:

$H^+ + e^- \leftrightarrow H_{ad}$ (Volmer) (1)

$2H_{ad} \leftrightarrow H_2$ (Tafel) (2)

$H_{ad} + H^+ + e^- \leftrightarrow H_2$ (Heyrovsky) (3)

In alkaline and neural solutions:

$H_2O + e^- \leftrightarrow H_{ad} + OH^-$ (Volmer) (4)

$2H_{ad} \leftrightarrow H_2$ (Tafel) (5)

$H_2O + H_{ad} + e^- \leftrightarrow H_2 + OH^-$ (Heyrovsky) (6)

Many researchers have confirmed that H_2 evolution rates are approximately two to three orders of magnitude slower in the alkaline media than that in the acidic media [27–29]. The exchange current density for Pt in the acidic media is about 200 mA cm^{-2}, while it is about 1.78 mA cm^{-2} in the alkaline media [27,28]. Compound-based catalysts, such as phosphides, sulfides, also have a larger overpotential in the alkaline media than that in the acidic media [29]. Durst *et al*. [15] supposed that the H atoms abstracted from H_2O instead of hydronium species (H_3O^+) induce the slow HER kinetics in alkaline solution. Strmcnik *et al*. [16] found that, in the pH range of 4 to11, pure diffusion-limiting currents are observed between certain applied potential ranges, which also depends on pH values. The current density plateau on the polarization curves implies that, under certain conditions, the HER is controlled by the mass transport of reactive H_3O^+, as shown in Figure 1a. However, such a level of understanding is not good enough to explain the phenomenon happening in the HER in the solutions with different pH values. For instance, why is the kinetics of the HER on platinum in alkaline media significantly slower than that in acidic media [30–32]? Why is there a steep increase of current signals after the plateau with increasing the applied overpotentials, even though the rate-determining step (RDS) is the mass transport of reactive hydronium species, which does not contribute enough to the sharply rising current density [16,33]? The macroscopic experiment results require the recognition from atomic-scale insights into water molecules for a fundamental understanding of the microscopic processes occurring in the HER [34–36]. In this review, we provide an overview of the atomic-scale activity descriptor of HER to understand how the water molecules affect the kinetics of HER. We conclude that water molecules change into reactants and accept electrons for hydrogen generation in certain applied-overpotentials when there are not enough hydronium species to afford the HER in the near-neutral electrolyte. And the interfacial water reorganization is essential to indicate the hydrogen evolution rate and can act as the dominant pH-dependent HER activity descriptor on platinum electrodes. A reasonable explanation for the HER is formed by discussing the interfacial water structure and water dissociation process.

2 The contribution of water molecules to the thermodynamic descriptor of HER

2.1 Hydrogen binding energy acting as a descriptor of HER

The differences in the kinetic rates of the HER on different electrodes have been occasionally correlated with the thermodynamic descriptors [31], the hydrogen adsorption energy or hydrogen binding energy (HBE) following the Sabatier principle, *i.e*., the proper bond strength between hydrogen and the metal electrode [37–40]. Several groups [15,41] have proposed that HBE can effectively explain alkaline HER activity trends as well, despite the complex nature of the elementary steps. As an early effort, Durst *et al*. [15] suggested that, for carbon-supported platinum-group metal catalysts (Pt/C, Ir/C, and Pd/C) and polycrystalline Pt, the significantly lower HER exchange current densities in alkaline media than those obtained in acidic media can be associated with HBE. Sheng *et al*. [19] found that the HBE increased linearly with the pH values. Then, they correlated the hydrogen oxidation and evolution activity, indicated by overpotential, on platinum electordes at different pH with HBE (Figure 1b, 1c). At present, the shifts of the voltammetric peaks corresponding to the underpotential deposition hydrogen region (H_{upd}) on polycrystalline platinum electrodes have been taken as a proof of such a pH-dependent HBE.

Meanwhile, according to Figure 1d, Markovic *et al*. [20] found that it was not possible to propose any correlation between the rate of the HER and the M–H bonding by categorizing metal electrodes into three distinct groups, *i.e*., the IB group (Cu, Ag, Au), the Pt group (Pt, Ir, Ru), and the 3d transition elements (V, Ti, Ni). Wang *et al*. [41] found that the HBE depended on the interaction of H atoms not only with the metal catalyst surface but also with the solution (electrolyte) species. They stated that the HBE depended on the thermodynamic property of the electrode/electrolyte interface by comparing the HBE of Pt, $Ru_1@Pt_1$ (2 monolayers (MLs)), and $Ru_1@Pt_{0.5}$ (1 ML) in acidic and alkaline media. Koper and coworkers [42] argued that the positive peak shift of the H_{upd} was not dependent on the pH but on the type of cations present in the electrolyte on Pt(553) surface. Koper *et al*. [43] recently suggested that the ‘hydrogen’ peak potentials on polycrystalline platinum were ambiguous indicators of HBE because the nature of the ‘hydrogen’ peaks was unlikely to be associated with the adsorption of hydrogen alone but also included the effect of the adsorption of oxygenated species on (110) and (100) sites.

Considering the presence of interfacial water, Yan *et al*.

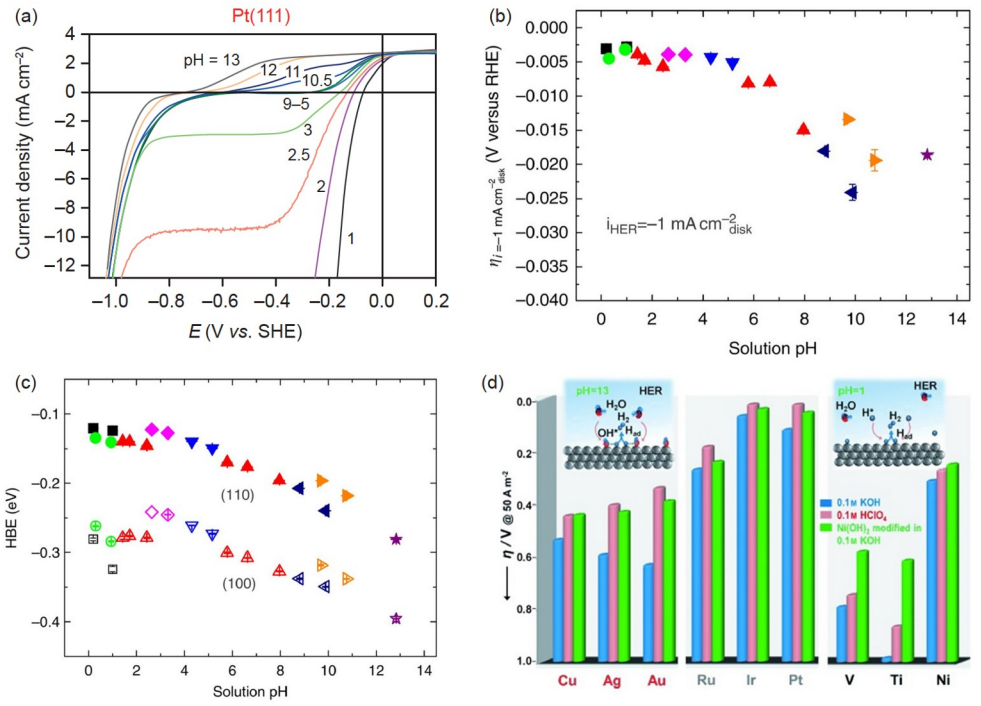

Figure 1 (a) Measured pH-dependent linear sweep voltammetry (LSV) curves at a rotation rate of 1,600 rpm and a sweep rate of 50 mV s^{-1} for a Pt(111) electrode. Reprinted from ref [16]. Copyright 2013 Springer Nature. (b) Overpotential of the HER on Pt at a current density of −1 mA cm^{-2} in all pH-buffered electrolytes. Reprinted from ref [19]. Copyright 2014 Springer Nature. (c) Hydrogen binding on Pt(110) (solid symbols) and Pt(100) (empty symbols) surface obtained from cyclic voltammetry (CV) curves as a function of pH in solution. Reprinted from ref [19]. Copyright 2014 Springer Nature. (d) Comparison between activities for the HER expressed as overpotential (η) required for a current density of 5 mA cm^{-2} in 0.1 mol L^{-1} $HClO_4$ and 0.1 mol L^{-1} KOH for both bare metal surfaces and $Ni(OH)_2$-modified surfaces. Metals are divided into three distinct groups: the IB group (Cu, Ag, Au), the Pt group (Pt, Ir, Ru), and the 3d transition-metal elements (V, Ti, Ni). Reprinted from ref [20]. Copyright 2012 John Wiley and Sons Ltd. (color online).

[44] proposed the apparent Gibbs free energy of hydrogen ($\Delta G^0_{H,app}$), which included the inherent HBE of the metal and the adsorption/desorption of water. The decreased HER activity for platinum-group metals with pH increase results from the weakened water adsorption. Goddard *et al.* [45] studied the adsorption of water and H on Pt(100) surface at different pH and potential by Quantum Mechanics Molecular Dynamics (QMMD) calculation. And they confirmed that, with the increase of pH and the negative shift of the potential, the Pt(100) surface repelled water and thus increased the adsorption of H, which may be the primary cause of the decrease of HER activity under alkaline conditions.

In the past few years, the fundamental understanding of the sluggish kinetics in alkaline media has mainly focused on the adsorption of the H intermediates [15,46], which enables the design and synthesis of catalysts to improve the slow kinetics of HER [47–51]. Nevertheless, a consistent explanation why the HER on Pt is slower in alkaline media than that in acidic media is still absent due to the limitations of the HBE theory for predicting the alkaline HER activity with several counter-examples. In addition to the HBE, recently, the favorable interaction of interfacial water and surface-adsorbed OH_{ads} has emerged to be considered in improving the kinetics of the HER [32,52], where the configuration and properties of water molecules are of vital importance. Hence, the donation of water molecules to the hydrogen evolution activity should be sorted out to disclose the kinetic of the HER in alkaline media.

2.2 Water molecules as reactants in HER

The fundamental understanding of the mechanism of HER has been mainly focused on two processes and three kinds of elementary steps [15,16,53]. In acidic electrolytes, the high proton concentration facilitates the generation of H_{ad} by protons adsorbing on the surface. The hydrogen combination, *i.e.*, the Tafel step, is generally thought to be the RDS, whereas, in alkaline and neutral electrolytes, HER is more complicated; both water dissociation (the Volmer step) and concomitant interaction of catalyst surface with the water dissociation products impact the overall reaction kinetics.

According to the electrode/electrolyte theory, water molecules are the few molecules that can enter the depth of the electrode/electrolyte interface because of a strong interaction between the charged electrode and water dipole. Its ionization equilibrium constant (K_c) is temperature-dependent as the equation (7). The concentration of water in solutions can be regarded as a constant. Hence, the ionization product constant of water (K_w) (8) is a constant at the determined temperature, and the K_w is 1.0×10^{-14} at 298 K. No matter in

acidic, alkaline, or neutral salt solutions, H_2O, H^+, and OH^- always follow the relationship governed by equation (7) and (8).

$$K_c = c(H^+)\cdot c(OH^-)/c(H_2O) \quad (7)$$

$$K_w = c(H^+)\cdot c(OH^-) \quad (8)$$

The molar ratios of both H_2O/OH^- and H_2O/H^+ in the aqueous solutions are shown in Table 1. On the electrode/electrolyte interface, the proportion of water molecules in all the investigated solutions is much larger than that of the proton and hydroxyl ions either in acidic or alkaline solutions. In extremely dilute acidic and alkaline solutions, such as 0.0001 mol L^{-1} $HClO_4$ and 0.0001 mol L^{-1} KOH, where the concentration of H^+ and OH^- ions is close to zero, water molecules naturally play a role of reactants in the HER on the cathode or the oxygen evolution reaction (OER) on the anode.

At the pH 1 and 2, the hydrogen-ion concentration is enough for hydrogen evolution. The kinetics of HER in different pH electrolytes has been researched from different perspectives. Mayrhofer *et al*. [33] investigated HER in different pH-buffered solutions. They found that the HER current in solutions with a pH-value between 4 and 10 exhibited a plateau in the potential interval between –0.25 and −0.55 V. Outside this potential region, a steep increase of the HER current *versus* the applied potential can be observed. Similar experimental results have also been obtained by Strmcnik *et al*. [16], implying that the HER is controlled by the mass transport of reactive hydronium species rather than the charge transfer reaction (Figure 1a). However, with increasing the applied cathodic potential, more questions emerge. Why is there a steep increase of current signals after the plateau at relatively high applied overpotentials, even though the RDS is the mass transport of reactive hydronium species, which does not contribute enough to the sharply increasing current density? What kinds of reactants do participate in hydrogen generation to increase the current density? A reasonable role of water as reactants and solvents in HER needs to be proposed to elucidate these questions.

In other words, the mass transport of reactive hydronium species can only preserve the current density of the plateau in the linear sweep voltammetry (LSV). With increasing the applied overpotential, the sharply rising current density in the near-neutral electrolyte indicates that there must be other reactants that accept electrons to facilitate the hydrogen evolution. Obviously, it is a water molecule that accepts electrons to generate hydrogen and then to contribute to the sharply increasing current density in the near-neutral electrolyte as long as the applied overpotential overcomes the energy barrier of water dissociation. Under alkaline conditions, as shown in Table 1, the molar ratio of water and H^+ is as high as 5.5×10^{14}:1 in 0.1 mol L^{-1} KOH. At this time, the possibility of proton participation in the reaction is extremely low, indicating that water molecules become the primary reactants to participate in the reaction directly. In addition,

Table 1 The molar ratio of H_2O/H^+ and H_2O/OH^- at different pH electrolytes

Electrolytes	The molar ratio of H_2O/H^+	The molar ratio of H_2O/OH^-
0.1 mol L^{-1} KOH	5.5×10^{14}	5.5×10^{2}
0.01 mol L^{-1} KOH	5.5×10^{13}	5.5×10^{3}
0.001 mol L^{-1} KOH	5.5×10^{12}	5.5×10^{4}
0.0001 mol L^{-1} KOH	5.5×10^{11}	5.5×10^{5}
0.1 mol L^{-1} $KClO_4$	5.5×10^{8}	5.5×10^{8}
0.0001 mol L^{-1} $HClO_4$	5.5×10^{5}	5.5×10^{11}
0.001 mol L^{-1} $HClO_4$	5.5×10^{4}	5.5×10^{12}
0.01 mol L^{-1} $HClO_4$	5.5×10^{3}	5.5×10^{13}
0.1 mol L^{-1} $HClO_4$	5.5×10^{2}	5.5×10^{14}

some researchers have confirmed the different kinetics under alkaline and acidic conditions through isotopic tracer technique, confirming the importance of interfacial water dynamics to HER [24,54].

Accordingly, more and more reports have confirmed the role of the water molecule as the reactant [54–56]. For instance, Grimaud *et al*. [55] investigated the role of interfacial water by using isolated water as the sole reactant in organic solvents. Combining experiments and molecular dynamics (MD) simulations, they observed that forming aqueous nanodomains, regulated by electrolyte cations, affects HER performance. Then, they emphasized that the long-range interaction between interfacial water was a key for HER. Xu *et al*. [56] also reported that the HER activity of Pt/C under the magnetic field across various pH remained unchanged. So they believed that the transport of protons had a weak effect on HER activity and emphasized that based on the Grotthuss transport mechanism, water could be used as a universal reactant for HER.

2.3 Water dissociation involving the hydroxide binding on the catalytic surface as descriptors for the HER

In neutral and alkaline solutions, water acts as a reactant to supply the source of hydrogen evolution. The continuous HER will be suppressed if water is weakly adsorbed on the catalyst surface and not provided timely [57–59]. Under alkaline conditions, the precious metal-based catalysts, such as Pt/C, show the highest intrinsic HER activity near the equilibrium potential compared with other transition-metal- and compound-based catalysts due to the optimum HBE [60]. However, at high overpotentials, some transition-metal- and compound-based catalysts exhibit a higher HER rate than the Pt/C catalyst because the sluggish water dissociation on Pt/C cannot match the fast formation of H_2 and then hinders the HER activity in the high polarization region [61]. Because water dissociation is the most critical step in alkaline HER, researchers take different views on the pathway of

water dissociation. Some believed that H_{ad} could be derived from the direct dissociation of adsorbed water [62–66], while others supposed that water molecules first changed into adsorbed hydroxyl-water-alkali metal cation (OH_{ad}–$(H_2O)_x$–AM^+) adducts.

The direct dissociation of adsorbed water to form H_{ad} and OH_{ad} is limited by the high energy barrier, which needs to be lowered by strengthening the H/OH adsorption on the catalyst surface [62–68]. Nevertheless, according to the Brønsted–Evans–Polanyi-type (BEP) theory [69], too strong adsorption of OH will cause reaction intermediates highly occupying the catalyst surface, then excluding the water adsorption. For this reason, appropriate OH_{ad} binding energy, that is, neither too strong nor too weak, is expected. Mo-doped Ni_3N has been proven to have favorite OH adsorption energy, thus boosting the alkaline HER with a low Tafel slope [70].

Markovic's group [32,71] initially proposed the bifunctional theory to spot the thermodynamic role of OH in alkaline HER. Markovic and coworkers suggested a delicate balance between the water dissociation and concomitant interaction of water dissociation products with the electrode surface. In the first step, water dissociation requires water adsorption. It is known that the polarized water molecules interact with each other through hydrogen bonds with the stabilization energies of 20–40 kJ mol^{-1} [74]; therefore, they tend to bind with each other rather than with the catalyst surface. If no strong hydrogen bonds or chemical interactions are formed between the electrode surface and water [75], which leads to the difficulty of water molecule activation, let the following reduction process alone. Adding $Ni(OH)_2$ to Pt can enhance the water adsorption by constructing a strong interaction between the water and hydroxyl ion. After that, the adsorbed water is dissociated into OH_{ad} and H_{ad} at the boundary between the Pt electrode and $Ni(OH)_2$ surface [16], where the edges of $Ni(OH)_2$ clusters promote the dissociation of water, and the Pt benefits the recombination of H_{ad}, showing the bifunctional effect [74].

The role of $M(OH)_2$ (M = Fe, Co, Ni, and Mn) cluster compositions on the alkaline HER has also been getting attention for many years. $Ni(OH)_2$ and $Co(OH)_2$ improved the alkaline HER performance, whereas $Fe(OH)_2$ and $Mn(OH)_2$ slowed down the HER kinetics (Figure 2b) [72], which was attributed to their different adsorption strength to OH_{ad}. Some reports suggested that the too strong adsorption of hydroxyl ions on the electrode surface could compete with water adsorption, consequently making alkaline HER kinetics slow down [76–78]. Motivated by these results, in conjunction with $M(OH)_2$ clusters, other oxophlic species (Ru, Rh, Ir, or *a*-MoC) have been proposed to stimulate the alkaline HER kinetics by adjusting the adsorption strength of OH_{ad} to improve water dissociation capability [79–82].

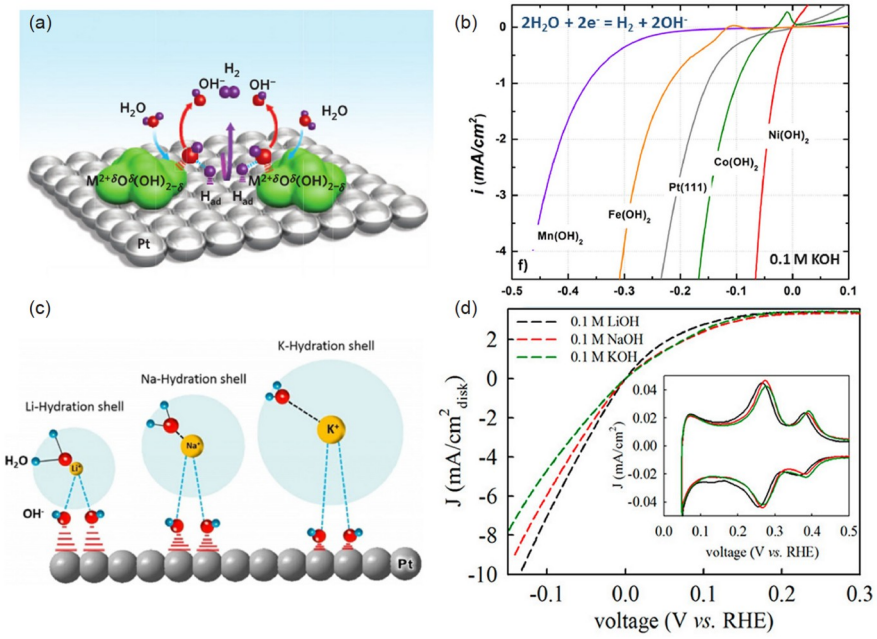

Figure 2 (a) Schematic diagram showing the HER. Water from the bulk of the electrolyte dissociatively adsorbs on the oxide cluster, forming the OH_{ad} intermediate on the oxide cluster, along with forming H_{ad} intermediates formed on the Pt substrate. The H_{ad} groups are re-combined to form H_2. Depending on the OH_{ad}–$M^{2+\delta}$ strength, the OH_{ad} is either stabilized (for Mn^{2+}, Fe^{2+}) or destabilized (Ni^{2+}, Co^{2+}) on the oxide clusters, which is found to dictate the turnover frequencies for these catalysts. Reprinted from ref [71]. Copyright 2012 Springer Nature. (b) HER polarization curves for Pt(111) surface modified with different transition metal hydroxides in a 0.1 mol L^{-1} KOH solution. Reprinted from ref [72]. Copyright 2018 John Wiley and Sons Ltd. (c) Schematic view describing the destabilization level of H–OH bonds of water and the increasing trend of the interaction between alkali metal cations and OH_{ad} on Pt surface in the presence of alkali metal cations with the order of K^+< Na^+< Li^+. Reprinted from ref [72]. Copyright 2018 John Wiley and Sons Ltd. (d) HER/HOR polarization curves of the polycrystalline Pt electrode in H_2-saturated 0.1 mol L^{-1} LiOH, NaOH, and KOH solutions. The inset in (d) presents the CV curves. Reprinted from ref [73]. Copyright 2019 American Chemical Society (color online).

The bifunctional mechanism of HER was well supported by our investigation [83]. In this study, DFT calculations on the H_2O dissociation step ($\Delta G(H_2O)$, Volmer step) and the H_{ad}-desorption step ($\Delta G(H)$, Tafel step) were performed on $NiMoPO_x$ and $Ni(OH)_2/NiMoPO_x$, respectively (Figure 3a). The energy change in the Volmer reaction (ΔG_R, Figure 3b) for $Ni(OH)_2/NiMoPO_x$ (0.60 eV) is lower than that for Ni^*MoPO_x (1.31 eV) and $Ni^*(OH)_2$ (1.38 eV), revealing that the $Ni^*(OH)_2/NiMoPO_x$ adduct is more favorable for H_2O dissociation thermodynamically. Moreover, the kinetic energy barrier (ΔG_{TS}) of water dissociation for $Ni^*(OH)_2/NiMoPO_x$ dramatically decreases from the 2.89 eV of Ni^*MoPO_x and 1.84 eV of $Ni(OH)_2$ to 1.01 eV, suggesting that the sluggish Volmer step on $NiMoPO_x$ was greatly accelerated with the participation of the $Ni(OH)_2$ component. As for the accompanying Tafel step (Figure 3c), the $Ni(OH)_2$ has a very negative $\Delta G(H)$ (−0.37 eV), indicating a too high H adsorption strength, while all these NiMoP-based catalysts present modulated $\Delta G(H)$ closer to the thermodynamic equilibrium. The $\Delta G(H)$ of Ni^*MoPO_x is further decreased by 0.04 eV when O atoms are doped into the Ni*MoP, suggesting that the incorporation of O can modulate the H adsorption on the surface of the NiMoP catalyst. Interestingly, the $Ni(OH)_2/Ni^*MoPO_x$ obtains an optimal $\Delta G(H)$ of 0.14 eV, which is even close to the absolute value of $\Delta G(H)$ for Pt* (0.09 eV) [84,85]. This research well supports the bifunctional mechanism of HER; that is, the two components in $Ni(OH)_2/NiMoPO_x$ could synergistically enhance water dissociation and hydrogen adsorption steps, respectively.

Nevertheless, the bifunctional mechanism of HER is still in question [86–89]. Tang *et al.* [88,89] disagree the bifunctional mechanism based on a rigorous kinetic study recently. In their research, the OH-mediated mechanism seems not to work for Pt(110) surface. They claimed that the OH slowed down the HER rate by behaving as a spectator that formed rapidly and thus reduced available catalytic sites, which indicated that only considering the thermodynamic adsorption energies of H and OH was insufficient for alkaline HER [88]. Because the addition of $M(OH)_2$ clusters into a catalyst likely induces electronic structural change (electronic effect) and the surface site covered. Using theoretical calculations, it is hard to model the state of $M(OH)_2$ cluster-mediated hydroxyl adsorption and transfer processes. Thus, they speculated that the way of OH influencing the reaction was more likely to be indirectly rather than directly participating in alkaline HER by analyzing the bifunctional case of Pt(111) with transition-metal surface clusters through single-crystal voltammetry and microkinetic modeling [89].

$$H_2O+(H_2O)_x–AM^+ \leftrightarrow H_{ad}+OH_{ad}–(H_2O)_x–AM^+ \quad (9)$$

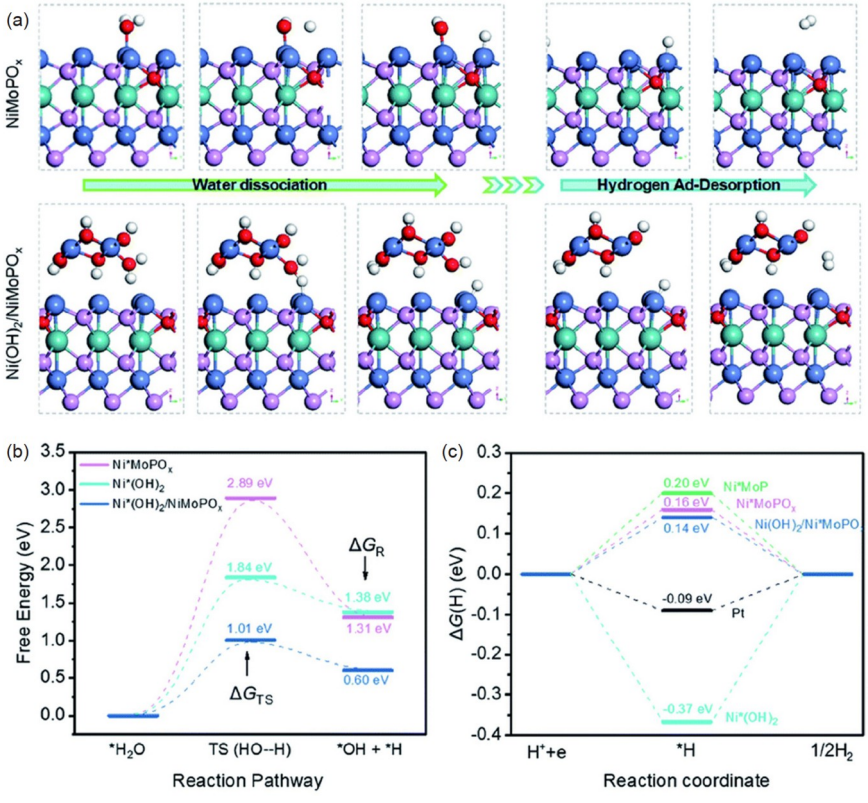

Figure 3 (a) Chemisorption models of H and OH intermediates on the surfaces of $NiMoPO_x$ and the $Ni(OH)_2/NiMoPO_x$ hybrid; calculated adsorption energy diagram of (b) the water dissociation step and (c) hydrogen ad-desorption for $Ni(OH)_2$, $NiMoPO_x$ and the $Ni(OH)_2/NiMoPO_x$ hybrid. The symbol * in the sample name represents the active site for DFT calculations. Color codes: Mo, cyan; P, pink; Ni, blue; O, red; H, white. Reprinted from ref [83]. Copyright 2020 Royal Society of Chemistry (color online).

OH_{ad}–$(H_2O)_x$–AM^++e^-↔OH^-–$(H_2O)_x$–AM^+ (10)

On the other hand, several ways have been proposed to describe the behavior of water molecules on the metal surface. It has been examined that water molecules are adsorbed directly on the bare Pd surface but adhered to the Pt surface through a chemically adsorbed hydrogen monolayer, whereas they are attached directly to the Au surface through hydrogen atoms [90]. Jia *et al*. [73] proved that water molecules first adsorbed on catalyst surface and turned into (OH_{ad})–water–alkali metal cation (AM^+) adducts, based on the observations of Pt/C, Pt_1Ni_1/C, and Ni/C electrodes in different concentrations of LiOH, NaOH, and KOH solutions. They divided the Volmer process (reaction (4)) in alkaline media into two steps, reaction (9) and (10). In line with the hard–soft acid–base (HSAB) theory, AM^+ is a hard Lewis acid, which binds strongly with the Lewis hard base OH^-, but weakly with soft Lewis base OH_{ad} with a nearly neutral charge [91]. Therefore, unbalanced binding energy originating from the unbalanced charge between OH^- and OH_{ad} promotes the migration of OH from the compact layer to the bulk electrolyte, thereby enhancing the Volmer step in HER. As a result, the presence of OH_{ad}–$(H_2O)_x$–AM^+ improves the HER, matching the enhanced HER selectivity of Pt/C and Pt_1Ni_1/C with increasing Li^+ concentration. It is known that AM–OH bond length increases in the order of LiOH<NaOH<KOH<CsOH; the hardness of Lewis acids decreases in the sequence Li^+>Na^+>K^+>Cs^+; the interaction energy between OH_{ad} and $(H_2O)_x$–AM^+ within OH_{ad}–$(H_2O)_x$–AM^+ increases, while the interaction energy between OH^- and $(H_2O)_x$–AM^+ within OH^-–$(H_2O)_x$–AM^+ decreases. Subsequently, the interaction energy gap between OH^-–$(H_2O)_x$–AM^+ and OH_{ad}–$(H_2O)_x$–AM^+ decreases as Li^+>Na^+>K^+ (Figure 2c) [72], and Li–water cluster should bind with OH weakly [92]. Thus, the driving force for the OH desorption decreases in the order Li^+>Na^+>K^+, matching the HER trend of LiOH>NaOH>KOH (Figure 2d) [73]. Oezaslan *et al*. [93] obtained a similar result. These researches indicated that the OH transfer (removal) process from the electrode surface was a rate-determining step. The OH–$(H_2O)_x$–AM^+ binding energy plays an important role in the alkaline HER.

As a result of the research method limitation, whether the H_{ad} forming from the adsorbed water or interfacial free water is still far from clear. However, in a certain way, the water dissociation process can boost the alkaline HER activity, or the OH adsorption energy is closely related to alkaline HER activity.

2.4 Reorganization of the interfacial water as a pH-dependent descriptor

Great efforts, especially the formation of the electrical double layer and the static and dynamic response of water molecules to the external electric field, have been made to understand the structural and dynamical properties of water adjacent to the catalyst surface [94], where electrocatalytic reactions take place [95,96]. Otani *et al*. [97] found that the water molecules formed a contact layer on the water/catalyst interface, *i.e*., the inner Helmholtz plane (IHP), which was the place that involved solvent molecules, reactants, products and reaction intermediates, and any other specifically adsorbed species [98]. In the IHP, water molecules near the catalyst surface, *i.e*., the interfacial water molecules, dissociate into intermediate adsorbed H_{ad} and OH_{ad} on the catalyst [99]. There is a dilemma for interfacial water molecules: the weak adsorption of water on catalysts gives rise to insufficient reactant supplement; on the other hand, strongly binding water molecules at IHP with large reorganization energy act as a kinetic barrier for the ion transport [100]. Interfacial water configuration and dynamic process are of high importance in determining the HER performance of catalysts [101], which may be modified by the applied electric field, the interfacial electric field [102–104], and the intrinsic characteristics of the electrocatalysts [105,106]. Only a deep understanding of interface water changes can better solve pH-dependence of HER activity [50,107–109].

Interfacial water at the electrode/electrolyte interface shows the different configurations with the change of applied electric fields. Nazmutdinov *et al*. [102] examined the water adsorption on a mercury cluster with an *ab initio* quantum chemical model. They found that adsorption energy varied approximately linearly with the electric field from 0.22 eV at 0.33 V $Å^{-1}$ to 0.33 eV at 0.46 V $Å^{-1}$. As shown in Figure 4a [97], when the surface is neutral, water is found to form a contact layer directing the O atoms toward the surface, *i.e*., O-down configuration (G1 geometry); when the surface is negatively biased, the O-down configuration is converted mostly to the H-down configuration (P2 peak, G2 geometry); for the weakly biased interface H^+ (−0.04 V), there is also an H-up configuration (P3 peak, G3 geometry). When the surface is biased more strongly, a hydrophobic double layer is formed in the contact layer (P4 peak, G4 geometry). The potential-dependent transformation of interfacial water configuration has also been confirmed by Li and Cheng's work [96]. Combined with *in situ* Raman spectra and *ab initio* molecular dynamics (AIMD), they found that, with a negative shift of potentials, the water in the interface underwent two structure transitions, from the "parallel" to "one-H-down" to the "two-H-down". At the same time, the number of hydrogen bonds in the interface network also changes. The width of the Helmholtz layer of the Pt(111)–H_{ad}/water interface becomes smaller when the potential shifts to the more negative direction due to increased electrostatic attraction between the charged surface and counterions [110]. It seemingly means that the strong interaction

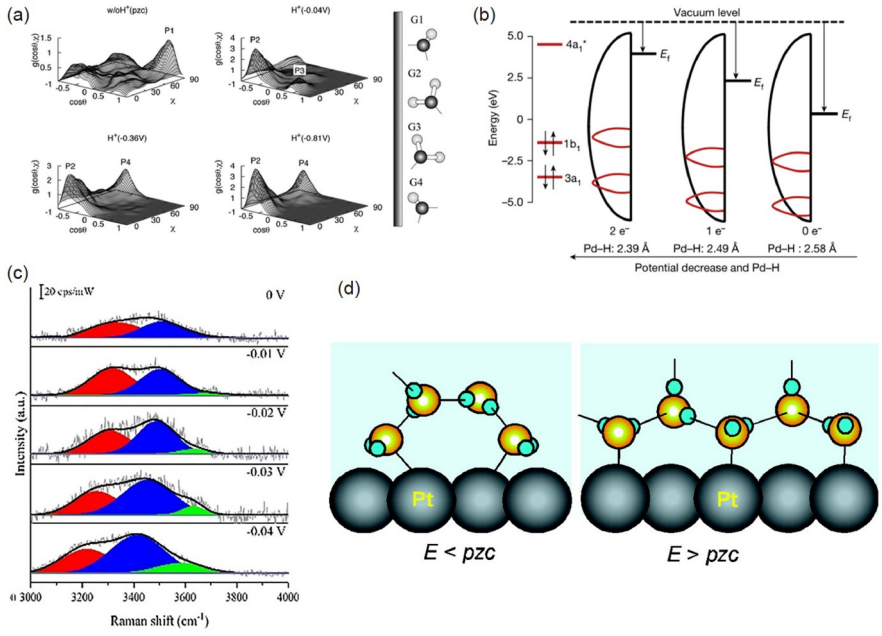

Figure 4 (a) Water molecule configurations for various orientations (cosθ, y, w). The black and gray spheres represent oxygen and hydrogen atoms, respectively. The thin sticks represent the lone pairs of electrons. The surface is located on the left of the water molecule. Reprinted from ref [97]. Copyright 2012 Royal Society of Chemistry. (b) Schematic showing the change in the density of states for the main orbital interactions between H_2O (red line) and the underneath Pd atom (black line) with decreasing potential using a Na·H_2O cluster model. Reprinted from ref [108]. Copyright 2021 Springer Nature. (c) *In situ* electrochemical Raman spectra at the $PtNi_{1.5}$ surface in 0.1 mol L^{-1} NaOH. Red: tetrahedrally coordinated water, blue: trihedrally coordinated water, and green: dangling O–H bonds of the interfacial water. Reprinted from ref [109]. Copyright 2020 John Wiley and Sons Ltd. (d) Schematic drawing of the possible water structures at the negatively (left) and positively (right) charged Pt surface, deduced from the surface-enhanced infrared absorption (SEIRA) spectra. Reprinted from ref [104]. Copyright 2008 American Chemical Society (color online).

between interfacial water and electrodes at a negative potential is inconsistent with the fact that the electrode tends to repel water molecule when the applied potential becomes more negative, resulting in weak water adsorption on the catalyst by a QMMD study [50]. Li *et al*. [108] found that under the cooperation of bias potential and hydrated cations, interface water molecules was observed from a random distribution to an ordered structure towards the Pd surface to promote the charge transfer across the interface to enhance the HER performance (Figure 4b), which was also directly proportional to the concentration and ionic strength of cations owing to the effect of interface electrostatic interaction.

Furthermore, Sun *et al*. [109] found that with increasing pH, the interfacial water structure on the electrode was also changed, and the change tendency was in agreement with that in the applied electric field (Figure 4c). They established the relationship between the HER rate and the interfacial water configuration. Under the alkaline condition, the activation energies of water dissociation increase in the order: the dangling OH bonds < the trihedrally coordinated water < the tetrahedrally coordinated water, the same order as the sequence of HER activity. Koper *et al*. [52,111] further proposed that the reorganization of interfacial water governed the HER activity. They found that, in alkaline solutions, a strong electric field existing at the electrode/electrolyte interfaces in the hydrogen region led to a large reorganization of H_2O when OH^- transfered through the double layer, which caused the hydrogen generation to be slow in alkaline media compared with that in acidic media. It is because, in acidic media, the potential of zero (free) charge (pzfc) of the Pt electrode is close to the HER equilibrium potential (0 V), whereas, in alkaline media, the pzfc of the Pt electrode is far from 0 V, which generates strong inner electric field at the electrode/electrolyte interface. They presumed that the electric field changing with increasing electrolyte pH slowed the reaction rate in alkaline solution owing to increased water reorganization energy. They also demonstrated the speculation by introducing $Ni(OH)_2$ onto Pt(111) to lower the pzfc on the electrode surface [111]. As a result, water becomes less rigid and is reorganized more easily (Figure 4d). It also means that the solution and the applied electrode potential-dependent interfacial water configuration dominate the water reorganization energy and dissociation kinetics and then can indicate the HER activity.

2.5 Coupling interfacial water's enrichment, reorientation, and dissociation

Given the increasing importance of interfacial water, coupling the water diffusion, interfacial water configuration, and water dissociation can significantly boost the HER kinetic activity. Our recent study also showed catalysts' composition

did change the water concentration on Pt/C and TiO_2–Pt/C by changing the surface electric field, as shown in Figure 5 [61]. The distribution of surface potential on the TiO_2–Pt/C electrode/electrolyte interface simulated by the finite-element method (FEM) was analyzed, as shown in Figure 5. During HER electrocatalysis, the catalyst surface is charged negatively due to the applied electrode potential. Compared with the Pt/C (Figure 5e), the TiO_2–Pt/C electrode/electrolyte interface possesses more negative surface potential (Figure 5a), showing a large electric field gradient due to the difference in relative permittivity between TiO_2 and Pt/C. In Figure 5c, the electric field gradient is extended to about 120 nm from the TiO_2 surface to the solution. And the induced electric field intensity on the TiO_2 surface is about -8×10^4 V m^{-1} as the applied electrode charge density of -1×10^{-4} C m^{-2}. The strengthened electric field gradient induced by metal oxides was named as local electric field enhancement (LEFE). When the charge density on the applied electrode increases to -2×10^{-4} C m^{-2}, the induced electric field intensity on the TiO_2 surface increases to -1.6×10^5 V m^{-1}, indicating that the LEFE on TiO_2–Pt/C electrode/electrolyte interface becomes more prominent. Correspondingly, the enhanced local electric field subsequently causes a noticeable hydrated K^+ ion enrichment. Figure 5b and 5d show that compared with the bulk solution, there are more hydrated K^+ ions with a concentration of about 40 and 80 mmol L^{-1} around the TiO_2 cluster at -1×10^{-4} and -2×10^{-4} C m^{-2} charge applied, respectively. That is, there are more H_2O molecules with concentrations of about 6×40 and 6×80 mmol L^{-1} around the TiO_2 cluster. However, the concentration of hydrated K^+ ions on pure Pt/C surface is almost the same as that in the bulk solution (Figure 5f). In a word, the LEFE induced by the introduction of TiO_2 further causes the enrichment of H_2O gathered around TiO_2, which is conducive to H_2O participation in the HER.

Meanwhile, the interfacial water orientation also appears to change from Pt/C to TiO_2–Pt/C, as shown in Figure 5g, which displays the statistical structure information of water around Pt(111) and TiO_2–Pt(111) surface. In the case of Pt (111) –KOH, the first peak of (H_2O)O–Pt and (H_2O)H–Pt, referring to the RDF of the first layer H_2O to Pt measured by O–Pt and H–Pt, respectively, appears at the distance of 2.12 Å for (H_2O)O–Pt and 2.68 Å for (H_2O)H–Pt. It means that most of the interfacial water molecules tend to interact with Pt by oxygen atoms instead of H atoms showing H-up structure, which is not conducive for subsequent H–O bond dissociation and H adsorption. By contrast, in the case of TiO_2–Pt(111) –KOH, although the orientation of interfacial water molecules on Pt is almost the same as that in the case of Pt(111)–KOH, the arranged pattern on TiO_2 is quite different, whereas interfacial water molecules are more tightly bound with Ti *via* two shorter distances, *i.e.*, 1.78 Å of (H_2O)H–TiO_2 and 1.88 Å of (H_2O)O–TiO_2. The shorter distances are more conducive for the subsequent H_2O activation than the two more prolonged distances in the case of Pt(111)–KOH. And the slightly shorter (H_2O)H–TiO_2 than (H_2O)O–TiO_2 means that the most interfacial water molecules exhibit an almost parallel structure with H slightly leaning to the TiO_2 surface.

Compared with Pt/C catalysts, the decoration of a small

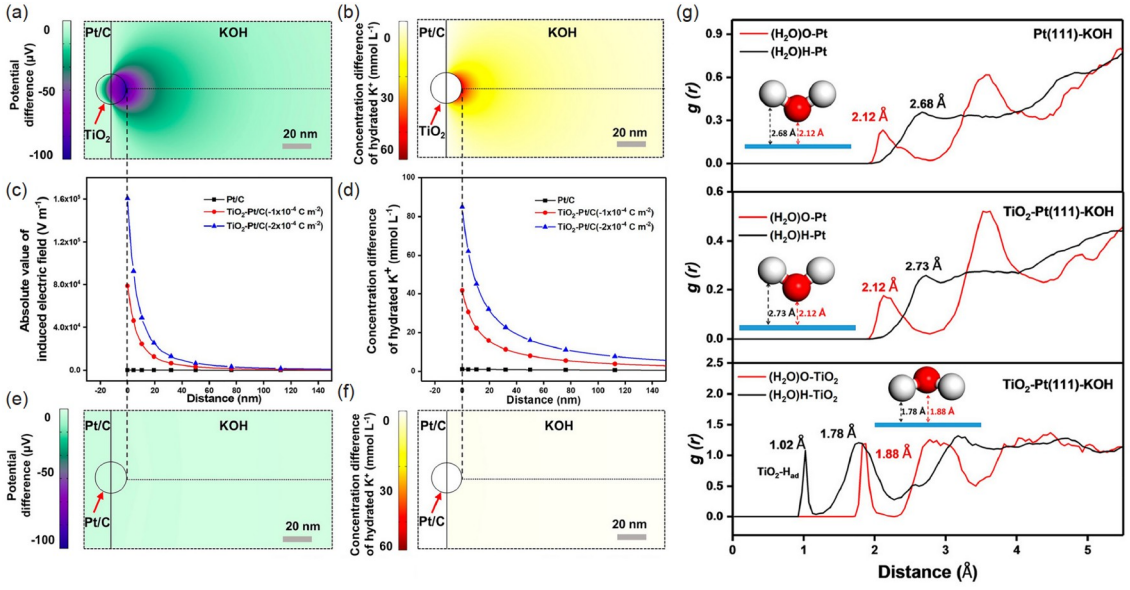

Figure 5 Simulated distribution of potential and hydrated K^+ concentration by the FEM for TiO_2–Pt/C ((a) and (b)) and Pt/C ((e) and (f)) at a charge density on the applied electrode of -1×10^{-4} C m^{-2}. The longitudinal distribution of (c) induced electric field and (d) hydrated K^+ concentration difference from electrode surface to bulk solution for TiO_2–Pt/C and Pt/C at a charge density on the applied electrode of -1×10^{-4} and -2×10^{-4} C m^{-2}, respectively. (g) The radial distribution function (RDF) of Pt(111)–water and TiO_2–water for Pt(111) and TiO_2–Pt(111) in KOH solution. The illustrations show the orientation of interfacial water. Reprinted from ref [61]. Copyright 2022 American Chemical Society (color online).

number of amorphous oxides, such as TiO_2, achieves better HER activity under the all polarization potential range by reducing the overpotential and Tafel slope. The metal oxides can cause local electric field enhancement to accelerate the diffusion of hydrated K^+ ions from the bulk solution to the electrode surface, especially near the metal oxide surface. In the IHP, the strong metal oxide–water interaction enriches more interfacial water and modulates water orientation as an H-down configuration to adapt to the subsequent water dissociation. And on the catalysts' surface, the metal oxides–Pt interface facilities the water dissociation and optimizes the H combination. The coupling of the above processes leads to a significant increase in the HER activity at a relatively wide polarization region, as shown in Figure 6 [61,112,113]. TiO_2–Pt/C catalysts exhibit an exceptional HER activity in alkaline conditions, delivering 10 and 500 mA cm^{-2} at an overpotential of 26 and 100 mV, respectively, surpassing almost all reported HER composite catalysts.

The above coupling-enhanced mechanism is also applicable for other metal- and metal compound-based composite catalysts. For example, the HER activities of Ni and CoP show a considerably increasing on the composite with MoO_2 and TiO_2 [114,115]. The reported HER activity of $MoNi_4$/MoO_2 catalysts exceeds that of commercial Pt/C catalysts [115]. Besides, many of the composite catalysts exhibit the higher HER activity at low and high current density, as shown in Figure 6c, indicating the universality of the coupling-enhanced mechanism [112–124]. Therefore, the influence of interfacial water's concentration, configuration, and orientation in the HER is definitive. Besides optimizing the HBE of the hydrogen–catalyst interaction, modulating the interfacial water configuration to boost the water dissociation and match the H recombination rate would be a more efficient way to improve HER kinetics in alkaline media.

3 Summary and outlook

In this review, we deeply discuss the role of water in the HER activity, in which water molecules not only act as solvents but serve as reactants involved in the alkaline HER. In HBE theory, the HBE corrected by considering water adsorption can well explain the different kinetic rates in alkaline and acidic media. The bifunctional theory reveals the one face of the water, in which water dissociation and followed H_{ad} and OH_{ad} desorption balance determine the HER activity. Furthermore, in IHP, the interfacial water configuration is

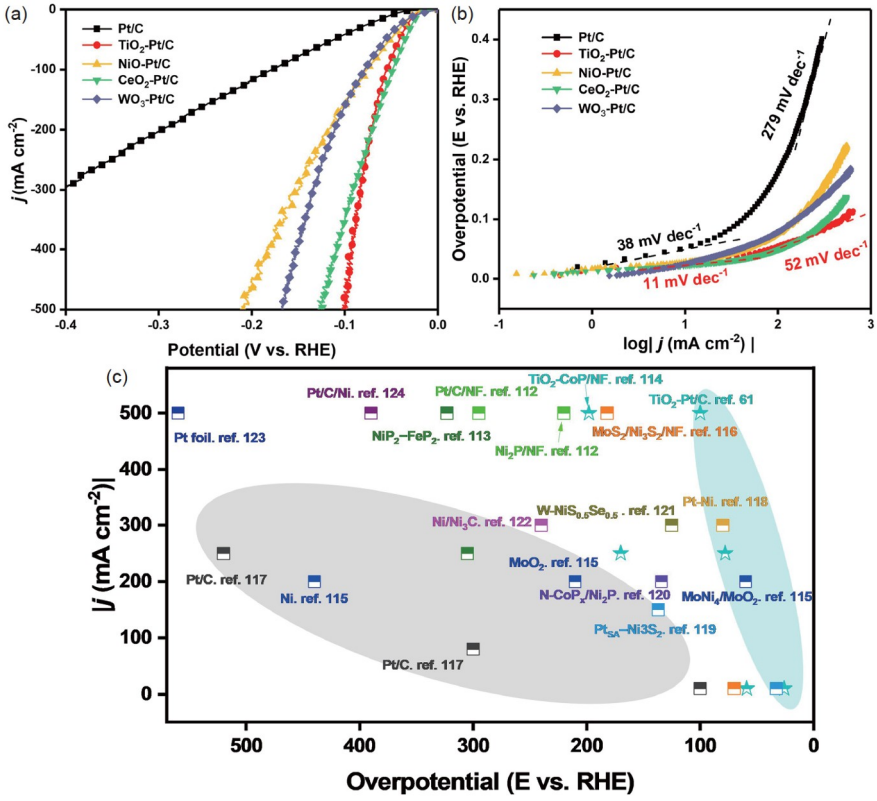

Figure 6 (a) The LSV curves of Pt/C, TiO_2–Pt/C, NiO–Pt/C, CeO_2–Pt/C, and WO_3–Pt/C. The LSV curves with a scan rate of 1 mV s^{-1} in 1 mol L^{-1} KOH with *iR* correction. The dotted lines represent the Ni_2P/NF [112] and NiP_2–FeP_2/Cu_{NW}/Cu_f [113] catalysts, respectively. (b) Corresponding Tafel plots for Pt/C, TiO_2–Pt/C, NiO–Pt/C, CeO_2–Pt/C, and WO_3–Pt/C. The dotted lines in (b) represent Tafel plots for Ni_2P/NF [112] and NiP_2−FeP_2/Cu_{NW}/Cu_f [113] catalysts, respectively. Reprinted from ref [61]. Copyright 2022 American Chemical Society. (c) Comparison of HER performance among the reported catalysts (The light green area represents the high current range, and the gray area represents the low current range) (color online).

thought to be critical to dominating the water dissociation rate by the different orientations of interfacial water, depending on the applied electrode potential, media, and catalyst compositions. Despite decades of development, there is still no consensus on how interfacial water affects HER. Based on the above discussion, to better understand the contribution of interfacial water molecules to the HER, we propose the following viewpoints.

Firstly, to delve into the complex processes of the water molecules' behavior in alkaline HER, advanced experimental tools can well capture reaction intermediates and offer an understanding of the reaction mechanism, such as *in situ* spectroscopic analyses, vibrational spectroscopy (infrared absorption spectroscopy, and sum-frequency generation spectroscopy), X-ray spectroscopy and isotope-labeling techniques.

Secondly, the reorganization of ion-solvated water molecules and hydronium ions at the electrode/electrolyte surface under the applied electric field should be more concentrated in the process of the HER. Molecular dynamics and coverage-dependent model studies, scanning electrochemical microscopy, and impedance spectroscopy are required in decoding local electrochemical behavior and minute surface changes. Meanwhile, developing and utilizing the high-precision computational chemistry methods will also facilitate understanding the interfacial water-related phenomena at the atomic scale.

Thirdly, there is a demand to establish a complete and clear reaction pathway, including the nonelectrochemical process, such as the mass transfer of solvated reactants, the reorientation and reorganization of solvent water molecules, and the electrochemical process, such as the electron and proton transfer, critical intermediate adsorption and desorption, and their impacts on HER. Considering the influence mechanism of the reaction from the overall pathway, the main factors can be more clearly determined, and the design criteria of targeted catalysts can be proposed.

Finally, a more complex solid–liquid interface should be considered and researched. Industrial water electrolysis uses 30 wt.%–40 wt.% KOH solution as the electrolyte and porous inorganic membranes as the separator; the electrochemical reaction occurs at the electrode/water interface. For anion exchange membranes (AEMs)-based electrolyzes, however, polymeric AEMs serve as the separator and solid electrolytes. The electrode/polymer/water interface becomes the essential location to afford the electrochemical reaction. And then, the electrode/polymer/water interface structure, composition, and amount are closely linked with the activity. A deep understanding of the solid–liquid interface can provide powerful theory and rational strategies to design electrodes and assemble electrolyzers with high performance.

Acknowledgements This work is financially supported by the National Key R&D Program (2021YFB4000301), the National Natural Science Foundation of China (22090030 and 52021004) and the Start-up Foundation of High-level Talents in Chongqing Technology and Business University (1956041 and 1952035).

Conflict of interest The authors declare no conflict of interest.

1 Seh ZW, Kibsgaard J, Dickens CF, Chorkendorff I, Nørskov JK, Jaramillo TF. *Science*, 2017, 355: eaad4998
2 Yang Y, Peltier CR, Zeng R, Schimmenti R, Li Q, Huang X, Yan Z, Potsi G, Selhorst R, Lu X, Xu W, Tader M, Soudackov AV, Zhang H, Krumov M, Murray E, Xu P, Hitt J, Xu L, Ko HY, Ernst BG, Bundschu C, Luo A, Markovich D, Hu M, He C, Wang H, Fang J, DiStasio Jr. RA, Kourkoutis LF, Singer A, Noonan KJT, Xiao L, Zhuang L, Pivovar BS, Zelenay P, Herrero E, Feliu JM, Suntivich J, Giannelis EP, Hammes-Schiffer S, Arias T, Mavrikakis M, Mallouk TE, Brock JD, Muller DA, DiSalvo FJ, Coates GW, Abruña HD. *Chem Rev*, 2022, 122: 6117–6321
3 Chi J, Yu H. *Chin J Catal*, 2018, 39: 390–394
4 Guo X, Wan X, Liu Q, Li Y, Li W, Shui J. *eScience*, 2022, 2: 304–310
5 Li M, Zheng X, Li L, Wei Z. *Acta Physico Chim Sin*, 2020, 36: 2007054
6 You N, Cao S, Huang M, Fan X, Shi K, Huang H, Chen Z, Yang Z, Zhang W. *Nano Mater Sci*, 2021, DOI:10.1016/j.nanoms.2021.05.004
7 Fang Y, Sun D, Niu S, Cai J, Zang Y, Wu Y, Zhu L, Xie Y, Liu Y, Zhu Z, Mosallanezhad A, Niu D, Lu Z, Shi J, Liu X, Rao D, Wang G, Qian Y. *Sci China Chem*, 2020, 63: 1563–1569
8 Wang F, Xu G, He Y, Liu Z, Zhang Z, Mao Q, Huang Y. *J Energy Chem*, 2020, 51: 101–104
9 Cheng C, Shah SSA, Najam T, Zhang L, Qi X, Wei Z. *J Energy Chem*, 2017, 26: 1245–1251
10 Zhang Z, Chen K, Zhao Q, Huang M, Ouyang X. *Nano Mater Sci*, 2021, 3: 89–94
11 Liu Q, Wang E, Sun G. *Chin J Catal*, 2020, 41: 574–591
12 Wang T, Cao X, Jiao L. *eScience*, 2021, 1: 69–74
13 Zhang S, Wu Y, Zhang YX, Niu Z. *Sci China Chem*, 2021, 64: 1908–1922
14 Li Z, Huang W. *Sci China Chem*, 2021, 64: 1076–1087
15 Durst J, Siebel A, Simon C, Hasché F, Herranz J, Gasteiger HA. *Energy Environ Sci*, 2014, 7: 2255–2260
16 Strmcnik D, Uchimura M, Wang C, Subbaraman R, Danilovic N, van der Vliet D, Paulikas AP, Stamenkovic VR, Markovic NM. *Nat Chem*, 2013, 5: 300–306
17 Schouten KJP, van der Niet MJTC, Koper MTM. *Phys Chem Chem Phys*, 2010, 12: 15217–15224
18 Fu C, Yan X, Yang L, Shen S, Luo L, Wei G, Zhang J. *Chin J Catal*, 2020, 41: 1698–1705
19 Sheng W, Zhuang Z, Gao M, Zheng J, Chen JG, Yan Y. *Nat Commun*, 2015, 6: 5848
20 Danilovic N, Subbaraman R, Strmcnik D, Chang KC, Paulikas AP, Stamenkovic VR, Markovic NM. *Angew Chem Int Ed*, 2012, 51: 12495–12498
21 Wang B, Huang H, Huang M, Yan P, Isimjan TT, Yang X. *Sci China Chem*, 2020, 63: 841–849
22 Wang Z, Shen K, Chen L, Li Y. *Sci China Chem*, 2022, 65: 619–629
23 Zhang Z, Ni L, Liu H, Zhao ZL, Yuan XZ, Li H. *Sci China Chem*, 2022, 65: 611–618
24 Sakaushi K. *Faraday Discuss*, 2020, 221: 428–448
25 Xue S, Garlyyev B, Watzele S, Liang Y, Fichtner J, Pohl MD, Bandarenka AS. *ChemElectroChem*, 2018, 5: 2326–2329
26 Jaksic M, Johansen B, Tunold R. *Int J Hydrogen Energy*, 1993, 18: 817–837
27 Zhou J, Zu Y, Bard AJ. *J Electroanal Chem*, 2000, 491: 22–29
28 Durst J, Simon C, Siebel A, Rheinländer PJ, Schuler T, Hanzlik M,

Herranz J, Hasché F, Gasteiger HA. *ECS Trans*, 2014, 64: 1069–1080
29 Wang J, Xu F, Jin H, Chen Y, Wang Y. *Adv Mater*, 2017, 29: 1605838
30 Conway BE, Bai L. *Electrochim Acta*, 1986, 31: 1013–1024
31 Sheng W, Gasteiger HA, Shao-Horn Y. *J Electrochem Soc*, 2010, 157: B1529
32 Subbaraman R, Tripkovic D, Strmcnik D, Chang KC, Uchimura M, Paulikas AP, Stamenkovic V, Markovic NM. *Science*, 2011, 334: 1256–1260
33 Auinger M, Katsounaros I, Meier JC, Klemm SO, Biedermann PU, Topalov AA, Rohwerder M, Mayrhofer KJJ. *Phys Chem Chem Phys*, 2011, 13: 16384–16394
34 Scatena LF, Brown MG, Richmond GL. *Science*, 2001, 292: 908–912
35 Chen YX, Zou SZ, Huang KQ, Tian ZQ. *J Raman Spectrosc*, 1998, 29: 749–756
36 Velasco-Velez JJ, Wu CH, Pascal TA, Wan LF, Guo J, Prendergast D, Salmeron M. *Science*, 2014, 346: 831–834
37 Laursen AB, Varela AS, Dionigi F, Fanchiu H, Miller C, Trinhammer OL, Rossmeisl J, Dahl S. *J Chem Educ*, 2012, 89: 1595–1599
38 Skúlason E, Tripkovic V, Björketun ME, Gudmundsdóttir S, Karlberg G, Rossmeisl J, Bligaard T, Jónsson H, Nørskov JK. *J Phys Chem C*, 2010, 114: 18182–18197
39 Zeradjanin AR, Polymeros G, Toparli C, Ledendecker M, Hodnik N, Erbe A, Rohwerder M, La Mantia F. *Phys Chem Chem Phys*, 2020, 22: 8768–8780
40 Yang B, Sharkas K, Gagliardi L, Truhlar DG. *Catal Sci Technol*, 2019, 9: 7003–7015
41 Elbert K, Hu J, Ma Z, Zhang Y, Chen G, An W, Liu P, Isaacs HS, Adzic RR, Wang JX. *ACS Catal*, 2015, 5: 6764–6772
42 Chen X, McCrum IT, Schwarz KA, Janik MJ, Koper MTM. *Angew Chem*, 2017, 129: 15221–15225
43 van der Niet MJTC, Garcia-Araez N, Hernández J, Feliu JM, Koper MTM. *Catal Today*, 2013, 202: 105–113
44 Zheng J, Nash J, Xu B, Yan Y. *J Electrochem Soc*, 2018, 165: H27–H29
45 Cheng T, Wang L, Merinov BV, Goddard III WA. *J Am Chem Soc*, 2018, 140: 7787–7790
46 Liu Y, Li W, Wu H, Lu S. *Acta Physico Chim Sin*, 2020, 0: 2009082–0
47 Zhang Q, Jiang Z, Tackett BM, Denny SR, Tian B, Chen X, Wang B, Chen JG. *ACS Catal*, 2019, 9: 2415–2422
48 Zhang Q, Tackett BM, Wu Q, Chen JG. *ChemElectroChem*, 2016, 3: 1686–1693
49 Michalsky R, Zhang YJ, Peterson AA. *ACS Catal*, 2014, 4: 1274–1278
50 Bouzid A, Pasquarello A. *J Phys Chem Lett*, 2018, 9: 1880–1884
51 Wei Y, Xu G, Wei Y, Ji L, Wang T, Liu Z, Wang S. *Sci China Mater*, 2022, doi:10.1007/s40843-022-2001-7
52 Ledezma-Yanez I, Wallace WDZ, Sebastián-Pascual P, Climent V, Feliu JM, Koper MTM. *Nat Energy*, 2017, 2: 17031
53 Gomez R, Fernandez-Vega A, Feliu JM, Aldaz A. *J Phys Chem*, 1993, 97: 4769–4776
54 Rebollar L, Intikhab S, Snyder JD, Tang MH. *J Phys Chem Lett*, 2020, 11: 2308–2313
55 Dubouis N, Serva A, Berthin R, Jeanmairet G, Porcheron B, Salager E, Salanne M, Grimaud A. *Nat Catal*, 2020, 3: 656–663
56 Wei C, Xu ZJ. *Chin J Catal*, 2022, 43: 148–157
57 Tian B, Gao W, Ning X, Wu Y, Lu G. *Appl Catal B-Environ*, 2019, 249: 138–146
58 Cai L, Lin Z, Wang M, Pan F, Chen J, Wang Y, Shen X, Chai Y. *J Mater Chem A*, 2017, 5: 24091–24097
59 Liu C, Gong T, Zhang J, Zheng X, Mao J, Liu H, Li Y, Hao Q. *Appl Catal B-Environ*, 2019, 262: 118245
60 Dubouis N, Grimaud A. *Chem Sci*, 2019, 10: 9165–9181
61 Deng M, Li M, Jiang S, Nie Y, Li L, Wei Z. *J Phys Chem Lett*, 2022, 13: 1069–1076
62 Zhao X, Zhang Z, Cao X, Hu J, Wu X, Ng AYR, Lu GP, Chen Z. *Appl Catal B-Environ*, 2020, 260: 118156
63 Zheng Y, Jiao Y, Vasileff A, Qiao SZ. *Angew Chem Int Ed*, 2017, 57: 7568–7579
64 Sun J, Xu W, Lv C, Zhang L, Shakouri M, Peng Y, Wang Q, Yang X, Yuan D, Huang M, Hu Y, Yang D, Zhang L. *Appl Catal B-Environ*, 2021, 286: 119882
65 Shang X, Zhang XY, Xie JY, Dong B, Chi JQ, Guo BY, Yang M, Chai YM, Liu CG. *Appl Catal B-Environ*, 2019, 258: 117984
66 Fu L, Yang F, Hu Y, Li Y, Chen S, Luo W. *Sci Bull*, 2020, 65: 1735–1742
67 Qin XP, Zhu SQ, Zhang LL, Sun SH, Shao MH. *J Electrochem*, 2021, 27: 185–194
68 Cheng PF, Feng T, Liu ZW, Wu DY, Yang J. *Chin J Catal*, 2019, 40: 1147–1152
69 Bligaard T, Nørskov JK, Dahl S, Matthiesen J, Christensen CH, Sehested J. *J Catal*, 2004, 224: 206–217
70 Zhang B, Wang J, Liu J, Zhang L, Wan H, Miao L, Jiang J. *ACS Catal*, 2019, 9: 9332–9338
71 Subbaraman R, Tripkovic D, Chang KC, Strmcnik D, Paulikas AP, Hirunsit P, Chan M, Greeley J, Stamenkovic V, Markovic NM. *Nat Mater*, 2012, 11: 550–557
72 Ruqia B, Choi SI. *ChemSusChem*, 2018, 11: 2643–2653
73 Liu E, Li J, Jiao L, Doan HTT, Liu Z, Zhao Z, Huang Y, Abraham KM, Mukerjee S, Jia Q. *J Am Chem Soc*, 2019, 141: 3232–3239
74 Luo Z, Zhang H, Yang Y, Wang X, Li Y, Jin Z, Jiang Z, Liu C, Xing W, Ge J. *Nat Commun*, 2020, 11: 1116
75 Israelachvili JN. *Q Rev Biol*, 2011, 2: 59–65
76 Yao M, Wang B, Sun B, Luo L, Chen Y, Wang J, Wang N, Komarneni S, Niu X, Hu W. *Appl Catal B-Environ*, 2021, 280: 119451
77 Gong M, Zhou W, Tsai MC, Zhou J, Guan M, Lin MC, Zhang B, Hu Y, Wang DY, Yang J, Pennycook SJ, Hwang BJ, Dai H. *Nat Commun*, 2014, 5: 4695
78 Strmcnik D, Lopes PP, Genorio B, Stamenkovic VR, Markovic NM. *Nano Energy*, 2016, 29: 29–36
79 Li Y, Guo Y, Yang S, Li Q, Chen S, Lu B, Zou H, Liu X, Tong X, Yang H. *ACS Appl Mater Interfaces*, 2021, 13: 5052–5060
80 Baek DS, Jung GY, Seo B, Kim JC, Lee HW, Shin TJ, Jeong HY, Kwak SK, Joo SH. *Adv Funct Mater*, 2019, 29: 1901217
81 Alinezhad A, Gloag L, Benedetti TM, Cheong S, Webster RF, Roelsgaard M, Iversen BB, Schuhmann W, Gooding JJ, Tilley RD. *J Am Chem Soc*, 2019, 141: 16202–16207
82 Li M, Duanmu K, Wan C, Cheng T, Zhang L, Dai S, Chen W, Zhao Z, Li P, Fei H, Zhu Y, Yu R, Luo J, Zang K, Lin Z, Ding M, Huang J, Sun H, Guo J, Pan X, Goddard III WA, Sautet P, Huang Y, Duan X. *Nat Catal*, 2019, 2: 495–503
83 Peng L, Liao M, Zheng X, Nie Y, Zhang L, Wang M, Xiang R, Wang J, Li L, Wei Z. *Chem Sci*, 2020, 11: 2487–2493
84 Liu T, Ma X, Liu D, Hao S, Du G, Ma Y, Asiri AM, Sun X, Chen L. *ACS Catal*, 2017, 7: 98–102
85 Liu T, Liu D, Qu F, Wang D, Zhang L, Ge R, Hao S, Ma Y, Du G, Asiri AM, Chen L, Sun X. *Adv Energy Mater*, 2017, 7: 1700020
86 McCrum IT, Koper MTM. *Nat Energy*, 2020, 5: 891–899
87 Chen Y, Wang X, Lao M, Rui K, Zheng X, Yu H, Ma J, Dou SX, Sun W. *Nano Energy*, 2019, 64: 103918
88 Intikhab S, Snyder JD, Tang MH. *ACS Catal*, 2017, 7: 8314–8319
89 Rebollar L, Intikhab S, Snyder JD, Tang MH. *J Electrochem Soc*, 2018, 165: J3209–J3221
90 Jiang YX, Li JF, Wu DY, Yang ZL, Ren B, Hu JW, Chow YL, Tian ZQ. *Chem Commun*, 2007, 4608–4610
91 Gázquez JL. *J Phys Chem A*, 1997, 101: 4657–4659
92 del Rosario JAD, Li G, Labata MFM, Ocon JD, Chuang PYA. *Appl Catal B-Environ*, 2021, 288: 119981
93 Weber DJ, Janssen M, Oezaslan M. *J Electrochem Soc*, 2019, 166: F66–F73
94 Guo J, Meng X, Chen J, Peng J, Sheng J, Li XZ, Xu L, Shi JR, Wang

E, Jiang Y. *Nat Mater*, 2014, 13: 184–189
95 Zhao X, Gunji T, Kaneko T, Yoshida Y, Takao S, Higashi K, Uruga T, He W, Liu J, Zou Z. *J Am Chem Soc*, 2019, 141: 8516–8526
96 Li CY, Le JB, Wang YH, Chen S, Yang ZL, Li JF, Cheng J, Tian ZQ. *Nat Mater*, 2019, 18: 697–701
97 Otani M, Hamada I, Sugino O, Morikawa Y, Okamoto Y, Ikeshoji T. *Phys Chem Chem Phys*, 2008, 10: 3609–3612
98 Dunwell M, Yan Y, Xu B. *Curr Opin Chem Eng*, 2018, 20: 151–158
99 Zheng J, Sheng W, Zhuang Z, Xu B, Yan Y. *Sci Adv*, 2016, 2: e1501602
100 Jiang Y, Huang J, Mao B, An T, Wang J, Cao M. *Appl Catal B-Environ*, 2021, 293: 120220
101 Liu E, Jiao L, Li J, Stracensky T, Sun Q, Mukerjee S, Jia Q. *Energy Environ Sci*, 2020, 13: 3064–3074
102 Nazmutdinov RR, Probst M, Heinzinger K. *J Electroanal Chem*, 1994, 369: 227–231
103 Garcia-Araez N, Climent V, Feliu J. *J Phys Chem C*, 2009, 113: 9290–9304
104 Osawa M, Tsushima M, Mogami H, Samjeské G, Yamakata A. *J Phys Chem C*, 2008, 112: 4248–4256
105 Intikhab S, Rebollar L, Fu X, Yue Q, Li Y, Kang Y, Tang MH, Snyder JD. *Nano Energy*, 2019, 64: 103963
106 García-Aráez N, Climent V, Feliu JM. *J Am Chem Soc*, 2008, 130: 3824–3833
107 Rossmeisl J, Chan K, Ahmed R, Tripković V, Björketun ME. *Phys Chem Chem Phys*, 2013, 15: 10321–10325
108 Wang YH, Zheng S, Yang WM, Zhou RY, He QF, Radjenovic P, Dong JC, Li S, Zheng J, Yang ZL, Attard G, Pan F, Tian ZQ, Li JF. *Nature*, 2021, 600: 81–85
109 Shen LF, Lu BA, Li YY, Liu J, Huang-Fu ZC, Peng H, Ye JY, Qu XM, Zhang JM, Li G, Cai WB, Jiang YX, Sun SG. *Angew Chem Int Ed*, 2020, 59: 22397–22402
110 Le JB, Chen A, Li L, Xiong JF, Lan J, Liu YP, Iannuzzi M, Cheng J. *JACS Au*, 2021, 1: 569–577
111 Sarabia FJ, Sebastián-Pascual P, Koper MTM, Climent V, Feliu JM. *ACS Appl Mater Interfaces*, 2019, 11: 613–623
112 Yu X, Yu ZY, Zhang XL, Zheng YR, Duan Y, Gao Q, Wu R, Sun B, Gao MR, Wang G, Yu SH. *J Am Chem Soc*, 2019, 141: 7537–7543
113 Kumar A, Bui VQ, Lee J, Jadhav AR, Hwang Y, Kim MG, Kawazoe Y, Lee H. *ACS Energy Lett*, 2021, 6: 354–363
114 Deng M, Yang H, Peng L, Zhang L, Tan L, He G, Shao M, Li L, Wei Z. *J Energy Chem*, 2022, 74: 111–120
115 Zhang J, Wang T, Liu P, Liao Z, Liu S, Zhuang X, Chen M, Zschech E, Feng X. *Nat Commun*, 2017, 8: 15437
116 Xue S, Liu Z, Ma C, Cheng HM, Ren W. *Sci Bull*, 2020, 65: 123–130
117 Liu W, Wang X, Wang F, Du K, Zhang Z, Guo Y, Yin H, Wang D. *Nat Commun*, 2021, 12: 6776
118 Nairan A, Liang C, Chiang SW, Wu Y, Zou P, Khan U, Liu W, Kang F, Guo S, Wu J, Yang C. *Energy Environ Sci*, 2021, 14: 1594–1601
119 Zhou KL, Han CB, Wang Z, Ke X, Wang C, Jin Y, Zhang Q, Liu J, Wang H, Yan H. *Adv Sci*, 2021, 8: 2100347
120 Wang L, gong N, Zhou Z, Zhang Q, Peng W, Li Y, Zhang F, Fan X. *Chin J Catal*, 2022, 43: 1176–1183
121 Wang Y, Li X, Zhang M, Zhang J, Chen Z, Zheng X, Tian Z, Zhao N, Han X, Zaghib K, Wang Y, Deng Y, Hu W. *Adv Mater*, 2022, 34: 2107053
122 Wen Q, Duan J, Wang W, Huang D, Liu Y, Shi Y, Fang JK, Nie A, Li H, Zhai T. *Angew Chem Int Ed*, 2022, 61: e202206077
123 Luo Y, Tang L, Khan U, Yu Q, Cheng HM, Zou X, Liu B. *Nat Commun*, 2019, 10: 269
124 Luo Y, Zhang Z, Yang F, Li J, Liu Z, Ren W, Zhang S, Liu B. *Energy Environ Sci*, 2021, 14: 4610–4619